ELSEVIER

Polymer 43 (2002) 3925–3936

polymer

www.elsevier.com/locate/polymer

Polymer-like structure of lecithin reverse micelles in the lecithin + water + cyclohexane system

Mika Kanamaru, Yoshiyuki Einaga*

Department of Chemistry, Nara Women's University, Nara 630-8506, Japan

Received 21 January 2002; received in revised form 7 March 2002; accepted 19 March 2002

Abstract

The lecithin reverse micelles with and without containing water in cyclohexane at 25.0 °C were characterized by static (SLS) and dynamic light scattering (DLS) experiments. The molar mass M^0 and hydrodynamic radius R_H^0 of the micelle determined at infinite dilution have increased with increasing water content W_0, demonstrating that the micelles grow in mass and in size with water uptake into them. The values of R_H^0 as a function of M^0 have been successfully analyzed with the use of the wormlike spherocylinder model. The results have revealed that the micelles with containing water assume a shape of rather flexible cylinders with the stiffness parameter $\lambda^{-1} = 11.0$ nm and the cross-sectional diameter $d = 5.2$ nm. It is also found that the intermolecular distance between hydrophobic tails of two adjacent lecithin molecules on the micellar surface is about 1.2 nm without regard to water content W_0. The micellar growth with increasing lecithin concentration has also been found to occur accompanying the structural evolution by combining information from SLS and DLS results.

Keywords: Lecithin micelle; Light scattering; Hydrodynamic radius

1. Introduction

The zwitterionic surfactant lecithin forms reverse micelles in organic solvents and the micelles grow in size with addition of relatively small amount of water. In the ternary phase diagram of the lecithin + organic solvent + water system, the micelle solutions form the isotropic water-in-oil microemulsion phase (L_2 phase) near the organic solvent apex of the phase triangle [1–3]. In particular, the L_2 phase of the lecithin + cyclohexane + water system spreads rather widely along the cyclohexane–lecithin axis from the cyclohexane apex [2,3]: lecithin can be dissolved in cyclohexane up to about 45 wt% and the binary micelle solutions can dissolve water up to a maximum of about 12 wt% depending upon lecithin concentration.

The micelles formed in the ternary systems have been characterized by various techniques such as static (SLS) and dynamic light scattering (DLS) [4–7], small angle neutron scattering (SANS) [1,8–10], rheological investigation [1,11–15], and so forth [2,3,16,17]. The rheological studies have revealed that the micelle solutions of sufficiently high lecithin and water content exhibit viscoelastic properties quite analogous to the behavior of concentrated polymer solutions, i.e. entangled polymer systems. In actuality, the dynamic storage modulus G' as a function of frequency for the highly concentrated solution exhibits the rubbery plateau region possibly due to the formation of a transient network consisting of cylindrical reverse micelles [1,12–15]. From the observations, it is supposed that the lecithin reverse micelles grow in size accompanying a structural change from spherical to rodlike or wormlike cylindrical shape with increasing lecithin concentration.

For the last decade, several attempts have been made to determine the size and structure of the micelles at dilute and semidilute regions in the L_2 phase by employing scattering techniques such as SLS, DLS, and SANS [4–10]. In practice, theoretical concepts and experimental methods highly developed in the polymer solution studies for this half century have been applied to the micelle solutions by treating the micelles as 'living' or 'equilibrium' polymers. Here, the term living or equilibrium is used in a sense that the linear macro-molecules formed with surfactant molecules can break and recombine. Although considerable efforts have been devoted to elucidation of the nature of the micelles, knowledge of the fundamental properties such as the micellar growth and structure is still insufficient at present. All the work done hitherto have been concerned with the micelle solutions at finite concentrations, in which concentration-dependent intermicellar interactions

* Corresponding author. Tel./fax: +81-742-20-3400.
E-mail address: einaga@cc.nara-wu.ac.jp (Y. Einaga).

0032-3861/02/$ - see front matter
PII: S0032-3861(02)00218-5

and micellar growth concomitantly occur. The contributions from both effects to the scattering results are not easily decoupled. Thus, the literature results obtained so far for the size, shape, and molar mass of the micelles are not necessarily unequivocal except for those on the local structure from the SANS measurements at large values of scattering vector, where the static structure factor is substantially independent of concentration.

In the present work, we have first characterized the lecithin reverse micelles in the L_2 phase at very dilute concentrations, where the micelles are isolated from each other without intermicellar interactions. To this end, we have extrapolated the mutual diffusion coefficient D obtained from DLS measurements and the osmotic compressibility $(\partial\pi/\partial c)_{T,p}$ from SLS measurements to infinite dilution of lecithin in order to remove the intermicellar interactions as in the usual case of polymer solution studies. Here, π is the osmotic pressure, c the lecithin concentration, T the absolute temperature, and p is the pressure. As to the extrapolation, some comments may be in order. One is that the micelles are formed at c higher than the critical micelle concentration (cmc) and physical properties of the solutions above and below cmc may be different from each other. All the present measurements have been done above cmc. Then, the extrapolation has been achieved not by following a possible variation of D or $(\partial\pi/\partial c)_{T,p}$ below or across the cmc but along a smooth line relevant to the micelle solutions to reach the value for the solution of micelles severed at infinite dilution. Secondly, the size, shape, and even molar mass M of the micelle may depend on the lecithin concentration c. Therefore, the solution properties may progressively vary with decreasing c in the course of the extrapolation and thus, a question may be raised as to if the state of the well-defined isolated-micelle solutions can be realized by the extrapolation. In advance of the results given below, we may say that we have obtained the positive answer to this question. In actuality, we have been able to successfully determine the hydrodynamic radius R_H^0 and molar mass M^0 of the lecithin reverse micelles at infinite dilution. We have also obtained the fundamental information on the micellar structure from the analysis of the relationship between R_H^0 and M^0 by using the wormlike spherocylinder model.

Following the characterization of the isolated lecithin reverse micelles, we have analyzed the micelle solutions at finite concentrations by combining information from the results by DLS and SLS measurements. It has been shown that the micelles grow and their shape evolve with increasing lecithin concentration c.

2. Experimental

2.1. Materials

Egg yolk lecithin (#20342) was supplied by Nacalai-Tesque Co. Ltd and used without further purification. The solvent cyclohexane was purified by distillation according to a standard procedure prior to use. The water used was also distilled water.

2.2. Dynamic light scattering

DLS measurements were carried out to determine the translational diffusion coefficient D for the lecithin reverse micelles with and without including water in cyclohexane at 25.0 °C by the use of a ALV DLS/SLS-5000/E light scattering photogoniometer and correlator system with vertically polarized incident light of 632.8 nm wavelength from a Uniphase Model 1145P He–Ne gas laser. The normalized autocorrelation function $g^{(2)}(t)$ of scattered light intensity $I(t)$, i.e.

$$g^{(2)}(t) = \langle I(0)I(t)\rangle/\langle I(0)\rangle^2 \tag{1}$$

was measured at scattering angles θ ranging from 30 to 150°.

The lecithin reverse micelle solutions were prepared by dissolving lecithin in cyclohexane with or without adding the appropriate amount of water with a microliter syringe (Hamilton). Complete mixing and micelle formation were achieved by stirring using a magnetic stirrer at least for one day. The solutions thus prepared were optically purified by filtration through a Teflon membrane of 0.22 μm pore size. The weight concentrations w of test solutions were determined gravimetrically and converted to mass concentrations c by the use of the densities ρ of the solutions given below. Throughout this paper, w and c denote the weight fraction and mass concentration of lecithin for the lecithin + cyclohexane binary solutions and those of lecithin + water for the lecithin + cyclohexane + water ternary solutions, respectively. In the latter case, the water content of a given solution is represented by the molar ratio W_0 of water to lecithin.

From the data for $g^{(2)}(t)$, we determined D by the equation [18,19]

$$(1/2)\ln[g^{(2)}(t) - 1] = (1/2)\ln f - K_1 t + \ldots \tag{2}$$

$$D = \lim_{q\to 0} K_1/q^2 \tag{3}$$

Here, f is the coherent factor fixed by the optical system, K_1 the first cumulant, and q is the magnitude of the scattering vector defined as

$$q = \frac{4\pi n}{\lambda_0}\sin(\theta/2) \tag{4}$$

with θ the scattering angle, λ_0 the wavelength of the incident light in vacuum, and n the refractive index of the solution. The values of D thus were extrapolated to $c = 0$ to obtain the infinite-dilution values D_0. It is to be noted that the D_0 values should be regarded as the z-average, since

lecithin reverse micelles observed may have distribution in size.

Some of the results for $g^{(2)}(t)$ were analyzed by the widely used program CONTIN [20] to examine distribution of the decay rate Γ; we have determined the distribution function $r(\Gamma)$ defined by

$$[g^{(2)}(t) - 1]^{1/2} = f^{1/2} \int_0^\infty r(\Gamma)\exp(-\Gamma t)\mathrm{d}\Gamma \quad (5)$$

2.3. Static light scattering

SLS measurements were performed to obtain $(\partial\pi/\partial c)_{T,p}$ and M from it for the binary and ternary micelle solutions at 25.0 °C with the same apparatus and light source as used in the DLS studies described earlier. For calibration of the apparatus, the intensity of light scattered from pure benzene was measured at 25.0 °C at a scattering angle of 90°, where the Rayleigh ratio $R_{Uv}(90)$ of pure benzene for unpolarized scattered light with polarized incident light at a wavelength of 632.8 nm was taken as 11.84×10^{-6} cm^{-1} [21,22].

All the test solutions studied are the same as those used in the DLS studies. The scattering intensities were measured for each solution and for the solvent cyclohexane at θ ranging from 30 to 150°. In all the present measurements, they were independent of θ or their angular dependence was negligibly small if any. Thus, the excess Rayleigh ratio ΔR_0 at zero scattering angle for a given solution was easily determined. From the data for ΔR_0, we evaluated $(\partial\pi/\partial c)_{T,p}$ by [23,24]

$$\frac{Kc}{\Delta R_0} = \frac{1}{RT}\left(\frac{\partial\pi}{\partial c}\right)_{T,p} \quad (6)$$

where R is the gas constant and K is the optical constant defined as

$$K = \frac{4\pi^2 n^2 (\partial n/\partial c)^2_{T,p}}{N_A \lambda_0^4} \quad (7)$$

with N_A the Avogadro's number and $(\partial n/\partial c)_{T,p}$ the refractive index increment. We note that the term on the right-hand-side of Eq. (6) gives an inverse of M at $c = 0$. Here, the value of M should be taken as a kind of average as is the case of D_0 mentioned earlier, although it is not explicitly indicated. It is also to be noted that in the present analyses, we treat the solutions consisting of lecithin, cyclohexane, and water as a substantially binary system by taking the lecithin reverse micelles including water as the solute component.

The value of $(\partial n/\partial c)_{T,p}$ was measured as a function of W_0 at 25.0 °C and at 632.8 nm with a Union Giken R601 differential refractometer. The results may be expressed by the equation

$$\left(\frac{\partial n}{\partial c}\right)_{T,p} = 0.0536 - 3.70 \times 10^{-3} W_0 + 1.02 \times 10^{-4} W_0^2 \quad (8)$$

for $c < 0.2$ g/cm^3.

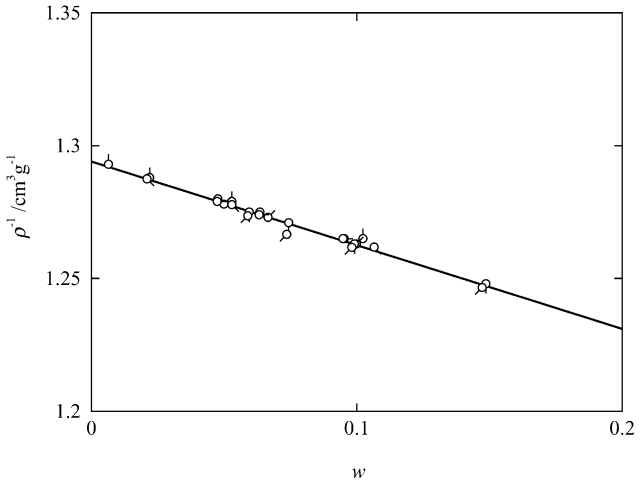

Fig. 1. Plots of ρ^{-1} against w for the micelle solutions with various W_0; pip up, $W_0 = 0$; pips with directions of successive clockwise 45° rotations correspond to $W_0 = 1.979$, 2.749, 2.906, 3.871, and 5.799, respectively. The solid straight line represents the values calculated by Eq. (9).

2.4. Density

The solution density ρ required for the calculation of c was measured at 25.0 °C with a pycnometer of the Lipkin–Davison type. In Fig. 1, ρ^{-1} is plotted against w for the micelle solutions of various W_0. The data points follow a straight line represented by

$$\rho^{-1} = 1.294 - 0.312w \quad (9)$$

irrespective of the value of W_0, as indicated.

2.5. Viscosity

Viscosity measurements were carried out for the micelle solutions at 25.0 °C by the use of conventional capillary viscometers of the Ubbelohde or Ostwald type. In all the measurements, the flow time was measured to a precision of 0.1 s, keeping the difference between flow times of the solvent cyclohexane and solution larger than ca. 20 s. The data obtained were treated by the Huggins and Fuoss–Mead plots to determine the intrinsic viscosity $[\eta]$. The test solutions were prepared in the same way as in the case of the DLS measurements described earlier.

3. Results

3.1. Diffusion coefficient

Fig. 2 shows examples of $g^{(2)}(t) - 1$ plotted against $\log t$ for the micelle solutions of lecithin weight fraction $w_{PC} = 0.0302$ g/cm^3 with various W_0 values indicated at scattering angle $\theta = 30°$. Here, w_{PC} is defined by $m_{PC}/(m_{PC} + m_{CH})$ with m_{PC} and m_{CH} being weights of lecithin and

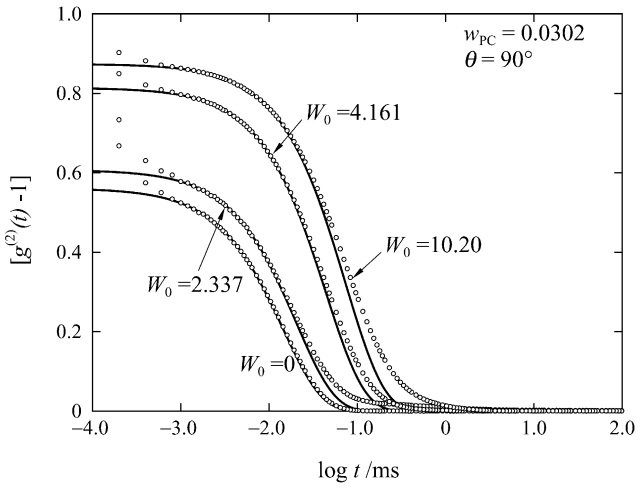

Fig. 2. Semi-logarithmic plots of $g^{(2)}(t) - 1$ against t for the micelle solutions of $w_{PC} = 0.0302$ and $W_0 = 0$, 2.337, 4.161, and 10.20 from left to right, respectively. The solid curves indicate the calculated values (see text).

cyclohexane, respectively. The solid curves represent the calculated results with single-exponential decay functions. The good agreement is found between the calculated and observed results for the solution with $W_0 = 0$. However, the data points for solutions with finite W_0 trail over the time axis longer than the corresponding calculations. The deviation of the data points from the calculated curve becomes larger as W_0 becomes larger, indicating the broader distribution of Γ for the larger W_0. Fig. 3 shows the results of the CONTIN analysis for the $g^{(2)}(t)$ data given in Fig. 2. In the case of $W_0 = 0$, a sharp peak appears at $\log \Gamma^{-1} \simeq -1.5$, indicating that the size distribution of the micelles in the solution is substantially monodisperse. As W_0 increases, the peak becomes broadened and shifted to longer time. Accompanying this, separate peaks appear at longer time region to some extent and their contribution to $r(\Gamma)$ becomes larger with increasing W_0. The results may imply that the distribution of the micelles in size and/or in shape becomes broad at large W_0. However, contribution of the main peak found at $\log \Gamma^{-1} \simeq -1.5$, or $\log \Gamma^{-1} \simeq -1$ to $r(\Gamma)$ remains dominant regardless of the values of W_0. An example of the concentration w dependence of $r(\Gamma)$ is shown for the micelle solutions with $W_0 \simeq 4$ in Fig. 4. It is found that $r(\Gamma)$ scarcely depends on w and the main peak at $\log \Gamma^{-1} \simeq -1$ dominantly contributes to $r(\Gamma)$ at any w, although a few peaks appear at longer time region. Thus, we may conclude that the micellar size and their distribution do not vary so much with w.

In Fig. 5, K_1 determined according to Eq. (2) is plotted against $\sin^2(\theta/2)$ for the solutions of $w_{PC} = 0.0505$ with

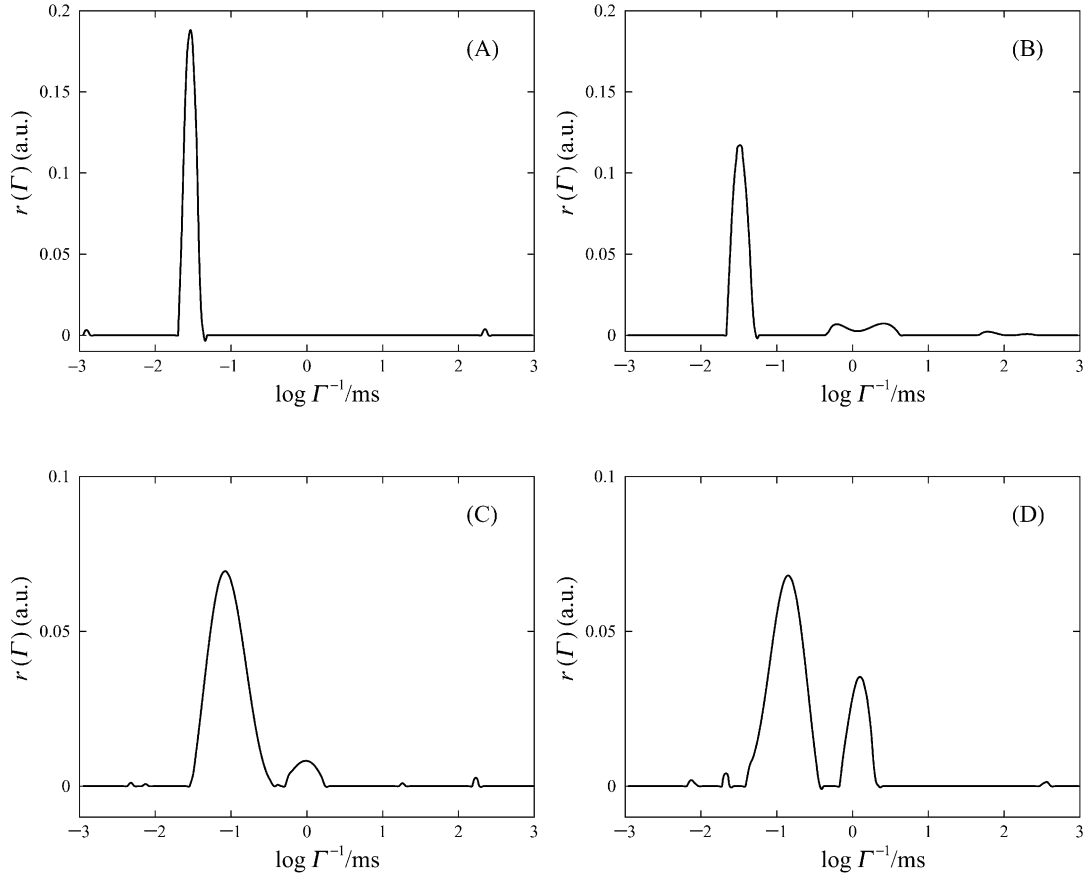

Fig. 3. W_0 dependence of $r(\Gamma)$ at $w = 0.0302$: (A) $W_0 = 0$; (B) $W_0 = 2.337$; (C) $W_0 = 4.161$; (D) $W_0 = 10.20$.

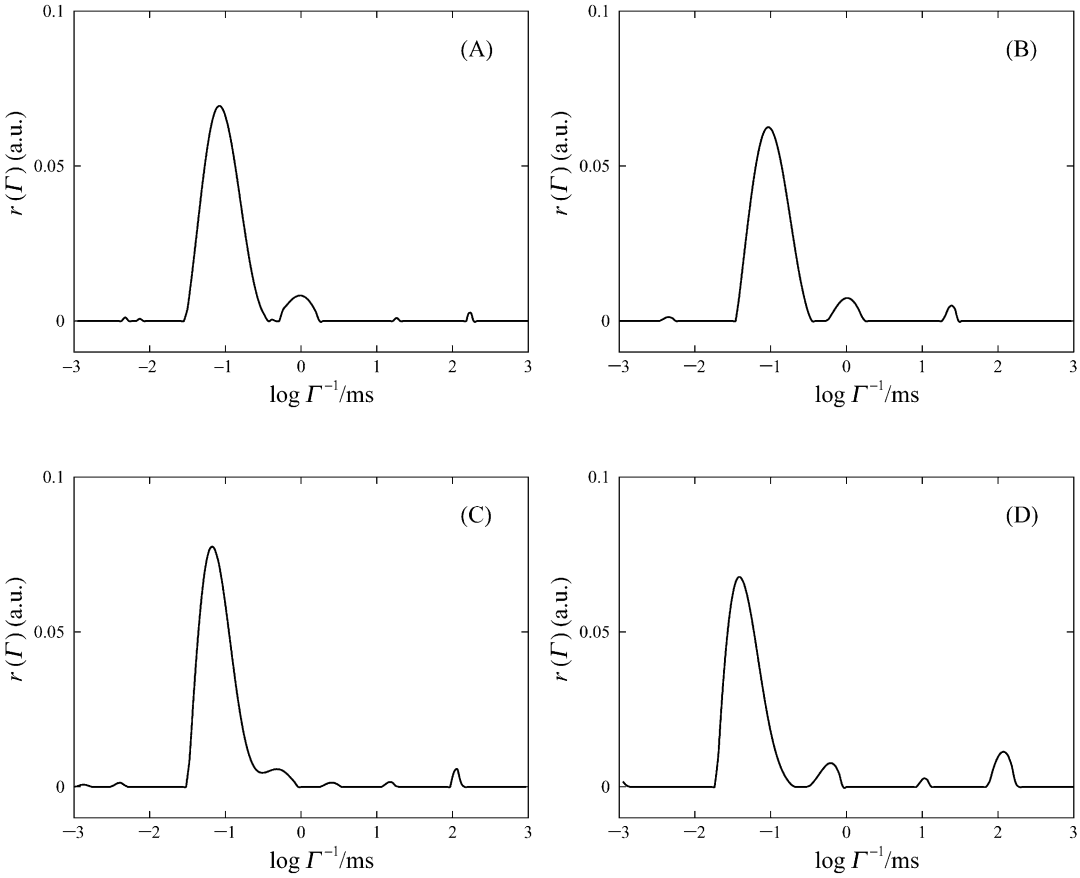

Fig. 4. Concentration dependence of $r(\Gamma)$: (A) $w = 0.0302$, $W_0 = 4.161$; (B) $w = 0.0505$, $W_0 = 4.105$; (C) $w = 0.1006$, $W_0 = 4.127$; (D) $w = 0.2007$, $W_0 = 4.016$.

various W_0. The data points for each W_0 closely follow a straight line passing through the origin, thereby permitting an accurate determination of D from its slope according to Eq. (3). Similar results as those in Fig. 5 have been obtained for all the micelle solutions examined, though they are not shown here.

In Fig. 6, all the values of D thus obtained are plotted against W_0 for the solutions with various fixed values of lecithin weight fraction w_{PC}. The data points at fixed w_{PC} follow a smooth curve concave upward as indicated, from which the values of D at fixed values of W_0 ranging from 0 to 10 have been evaluated as a function of w_{PC}. Fig. 7 depicts plots of the values of D thus determined against c, the points representing the values for $W_0 = 0$, 1, 2, 3, 4, 5, 6, 8, and 10 from top to bottom. Here, c has been calculated from the values of W_0 and w_{PC} in combination with Eq. (9). The data points for respective W_0 are seen to follow smooth curves slightly bent upward. We may then determine the value of D at $c = 0$, i.e. D_0, easily from the ordinate intercept, as indicated. As mentioned in Section 1, we have ignored the possible change in the concentration dependence of D at cmc which is undoubtedly located in between $c = 0$ and the lowest c examined. The values of D_0 obtained are given in Table 1.

We may define the hydrodynamic radius R_H^0 from D_0 as

$$R_H^0 = \frac{k_B T}{6\pi\eta_0 D_0} \tag{10}$$

with k_B the Boltzmann constant and η_0 the solvent viscosity. The values of R_H^0 calculated from those of D_0 by Eq. (10) are also summarized in Table 1 and plotted against W_0 in Fig. 8. Here, the value of η_0 we used for the solvent cyclohexane at 25.0 °C is 0.898 cP [25]. They are found to increase following a sigmoidal curve with increasing W_0, suggesting that

Table 1
Values of D_0, R_H^0, M^0, and n_{PC} for lecithin reverse micelles

W_0	D_0 (cm^2/s)	R_H^0 (nm)	$10^{-4}M^0$	n_{PC}
0	7.45×10^{-7}	3.26	5.41	74
1	5.55×10^{-7}	4.38	9.18	122
2	4.22×10^{-7}	5.76	16.7	217
3	3.02×10^{-7}	8.05	30.9	392
4	2.30×10^{-7}	10.6	51.0	632
5	1.95×10^{-7}	12.6	74.3	902
6	1.72×10^{-7}	14.1	108	1280
8	1.55×10^{-7}	15.7	160	1820
10	1.57×10^{-7}	15.5	173	1890

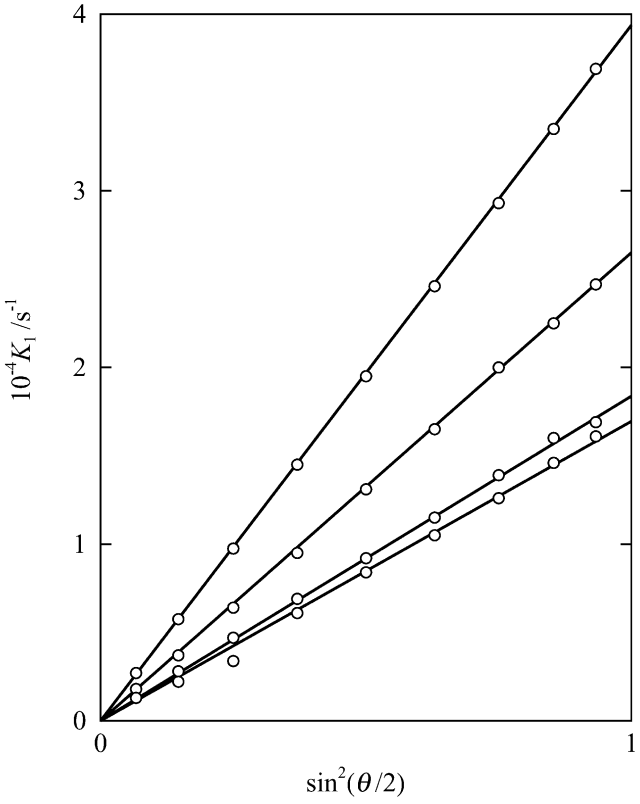

Fig. 5. Plots of K_1 against $\sin^2(\theta/2)$ for the micelle solutions of $w_{PC} = 0.0505$ with various W_0; the values of W_0 are 2.250, 3.407, 5.197, and 8.082 from top to bottom, respectively.

the micelles continuously grow in size by the incorporation of larger amount of water into them.

3.2. Molar mass of micelles

The values of $Kc/\Delta R_0$ for all the micelle solutions examined at various w_{PC} are plotted in the form of $(Kc/\Delta R_0)^{1/2}$ vs. W_0 in Fig. 9. At fixed w_{PC}, $(Kc/\Delta R_0)^{1/2}$ decreases rather steeply at first, passes through a shallow minimum, and then gradually increases as W_0 increases. We have determined the value of $Kc/\Delta R_0$ at fixed W_0 ranging from 0 to 10 as a function of w_{PC} from the smooth curve fitted to the data set for fixed w_{PC}. The values of square-root of $Kc/\Delta R_0$ thus evaluated at fixed W_0 are plotted against c in Fig. 10 as in the case of D shown in Fig. 7. The data points for each W_0 approximately follow a straight line at small c and are thus easily extrapolated to the value at $c = 0$. The c dependence of $Kc/\Delta R_0$ is often interpreted in terms of the polymer solution theory represented as

$$\frac{Kc}{\Delta R_0} = \frac{1}{M} + 2A_2c + \ldots \tag{11}$$

which is derived from Eq. (6). Here, A_2 is the second virial coefficient. However, as stated in Section 1, the molar mass

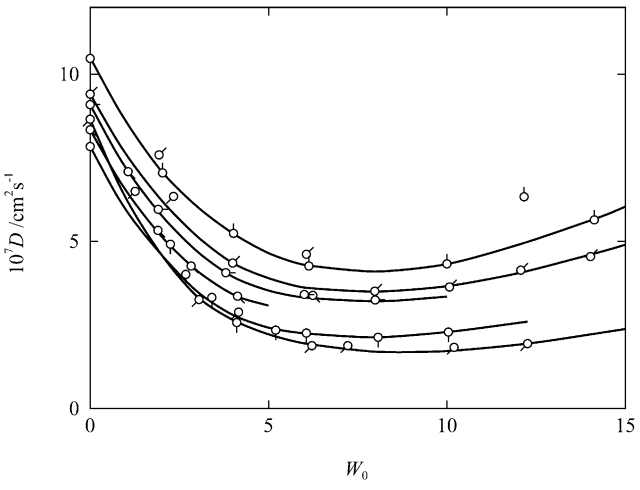

Fig. 6. Plots of D against W_0 for the micelle solutions of various w_{PC}; pip up, $w_{PC} = 0.2007$ pips with directions of successive clockwise 45° rotations correspond to $w_{PC} = 0.1506$, 0.1306, 0.1006, 0.0505, and 0.0302, respectively.

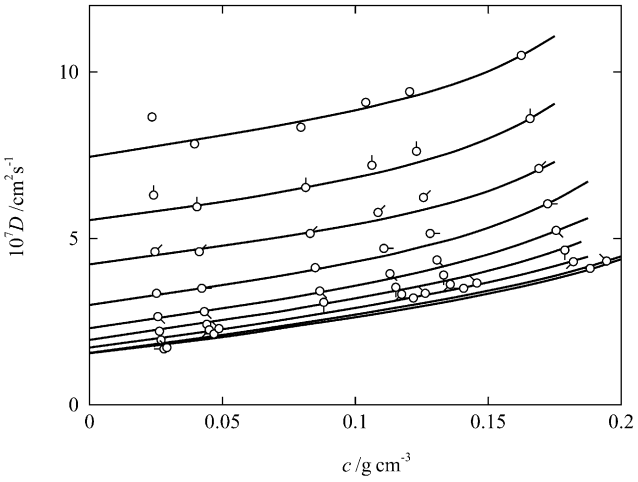

Fig. 7. Plots of D against c for the micelle solutions with various W_0; no pip, $W_0 = 0$; pip up, $W_0 = 1$; pips with directions of successive clockwise 45° rotations correspond to $W_0 = 2$, 3, 4, 5, 6, 8, and 10, respectively.

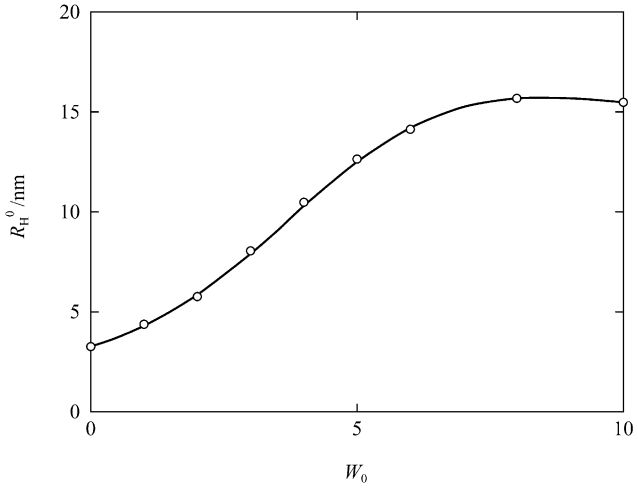

Fig. 8. Plots of R_H^0 against W_0. The solid curve is merely to guide the eye.

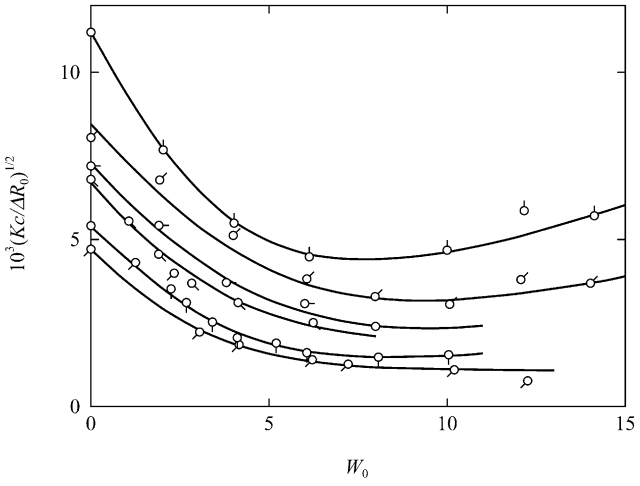

Fig. 9. Plots of $(Kc/\Delta R_0)^{1/2}$ against W_0 for the micelle solutions of various w_{PC}. Symbols have the same meaning as those in Fig. 6.

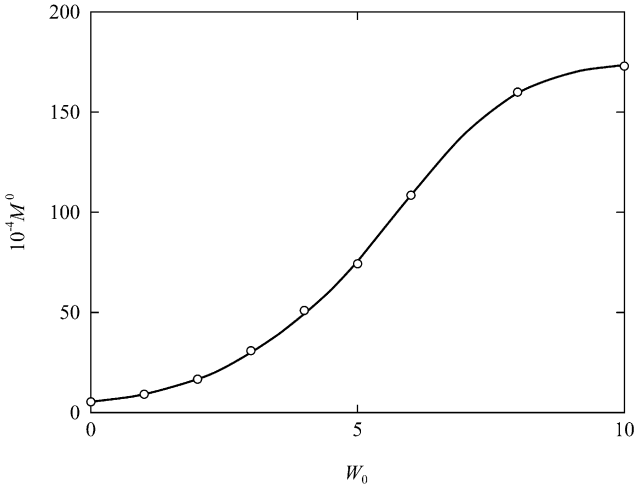

Fig. 11. Plots of M^0 against W_0. The solid curve is merely to guide the eye.

M of the micelle may vary with concentration in the micelle solutions, being different from the case of polymer solutions. It is thus considered that the c dependence of $(Kc/\Delta R_0)^{1/2}$ found in Fig. 10 does not necessarily reflect only the values of virial coefficients such as A_2 and so on, but possibly includes the effect of concentration-dependent increase of M. From this point of view, we have determined only the values of the molar mass of the micelles M^0 at infinite dilution from the ordinate intercepts of the lines drawn in Fig. 10. The values of M^0 obtained are given in Table 1 along with those of D_0 and R_H^0, and plotted against W_0 in Fig. 11. The number n_{PC} of lecithin molecules containing in the micelle is calculated from the values of M^0 and W_0 together with that of molecular weight of lecithin 734, as shown in Table 1.

It is found from Fig. 11 that the lecithin reverse micelle grows with increasing W_0 following a sigmoidal curve similar to that of R_H^0, shown in Fig. 8. The results indicate that the micelle grows by including water in it until the value of M^0 reaches up to about 30 times that of the micelle at $W_0 = 0$, i.e. in the lecithin + cyclohexane binary solutions. As is the case with R_H^0 shown in Fig. 8, M^0 tends to level off at large W_0. The results suggest that the solution approaches the boundary of the L_2 phase with increasing W_0 and the micelle takes limiting maximum size near the phase boundary.

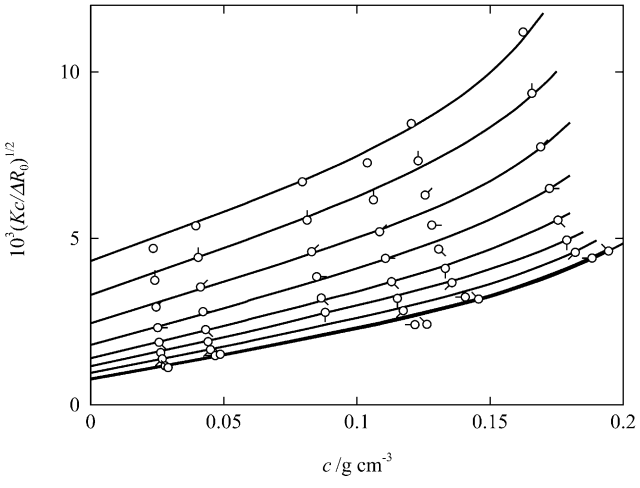

Fig. 10. Plots of $(Kc/\Delta R_0)^{1/2}$ against c for the micelle solutions with various W_0. Symbols have the same meaning as those in Fig. 7.

3.3. Intrinsic viscosity

Results for the intrinsic viscosity $[\eta]$ for the lecithin reverse micelles in cyclohexane at 25.0 °C are summarized in Table 2. When we use the Einstein intrinsic viscosity $[\eta]_E$ for rigid spheres, which reads

$$[\eta]_E = \frac{10\pi N_A a^3}{3M_s} \tag{12}$$

with a and M_s being the radius and molar mass of the sphere, respectively, we obtain 3.11 nm for a for the micelle in the binary solution with $W_0 = 0$ by using the value of $[\eta]$ in Table 2 for $[\eta]_E$ and that of M^0 in Table 1 for M_s. This value of a is in close agreement with that of R_H^0 given in Table 1. The result strongly suggests that the micelle at $W_0 = 0$ assumes a rigid spherical shape in the infinitely dilute state. Further discussion on the micellar growth with

Table 2
Values of $[\eta]$ for lecithin reverse micelles

W_0	$[\eta]$ (ml/g)
0	3.52
2.565	3.82
2.971	4.89
3.871	9.40
4.802	14.6
5.799	17.4
7.899	10.2

increasing W_0 which is derived from the data in Table 2 is given later.

4. Discussion

4.1. Molar mass M^0 dependence of hydrodynamic radius R_H^0

In order to elucidate the shape evolution of the lecithin reverse micelles caused by water uptake at infinite dilution, we first compare the present results for the M^0 dependence of R_H^0 with theoretical calculations for rigid particles such as sphere, prolate and oblate ellipsoids. For the rigid sphere model, R_H^0 is equal to its radius a, and those for the prolate and oblate ellipsoid models are given as [26]

$$R_H^0 = \frac{R_e(P^2-1)^{1/2}}{P^{1/3}\ln[P+(P^2-1)^{1/2}]} \qquad \text{(prolate ellipsoid)} \tag{13a}$$

$$R_H^0 = \frac{R_e(P^2-1)^{1/2}}{P^{2/3}\tan^{-1}(P^2-1)^{1/2}} \qquad \text{(oblate ellipsoid)} \tag{13b}$$

Here P is the axial ratio of the ellipsoid, i.e. the major radius divided by the minor one and R_e is the radius of a sphere equal in volume to the ellipsoid. In turn, R_e is represented as

$$R_e = P^{1/3}b \qquad \text{(prolate ellipsoid)} \tag{14a}$$

$$R_e = P^{2/3}b \qquad \text{(oblate ellipsoid)} \tag{14b}$$

with b the minor radius of the ellipsoid.

In the present work, we have converted the axial ratio P of the ellipsoid to its molar mass M^0 by using the relation

$$\frac{4\pi R_e^3}{3} = \frac{M^0 v}{N_A} \tag{15}$$

with v being the specific volume of the rigid particle. Note that the radius a of the rigid sphere may be converted to M^0 by Eq. (15) with a taking the place of R_e.

Fig. 12 depicts double-logarithmic plots of R_H^0/R_H^* against M^0/M^* for the present data (unfilled circles) given in Table 1 and for the theoretical values calculated for sphere (dashed line), prolate (dot-dashed curve) and oblate (dotted curve) ellipsoids, where R_H^* and M^* denote, respectively, the values of R_H^0 and M^0 for the rigid sphere. Note that the lecithin reverse micelle assumes a spherical shape at $W_0 = 0$ as stated earlier. In the theoretical calculations for the ellipsoids, the values of b and v are taken to be independent of P, and the former is set equal to a. The assumption about v is in line with the present finding that v is independent of W_0 as shown in Fig. 1. In Fig. 12, the data points clearly deviate upward from the dashed straight line for the rigid sphere progressively with increasing M^0/M^*, or in other words, with increasing W_0, except for the one at the origin. They are rather close to the values expected for the prolate ellipsoids at M^0/M^* values smaller than ca. 15 and then deviate downward from the latter at larger M^0/M^*. Accordingly, the prolate ellipsoid model, which is substantially the same as a rigid rod model, cannot explain the present results over the whole range of M^0. It is suggested that the lecithin reverse micelles change their shape from sphere to prolate ellipsoid or cylindrical shape, and the ellipsoidal or the cylindrical micelles become bent more significantly as M^0/M^* becomes larger, i.e. as the micelles become longer. This picture of the micellar shape is analogous to the one inferred by the previous authors [4–6,8,9] for the micelles in the same system at finite concentrations. On the basis of this finding, we analyze the present data by using a wormlike spherocylinder model in Section 4.2.

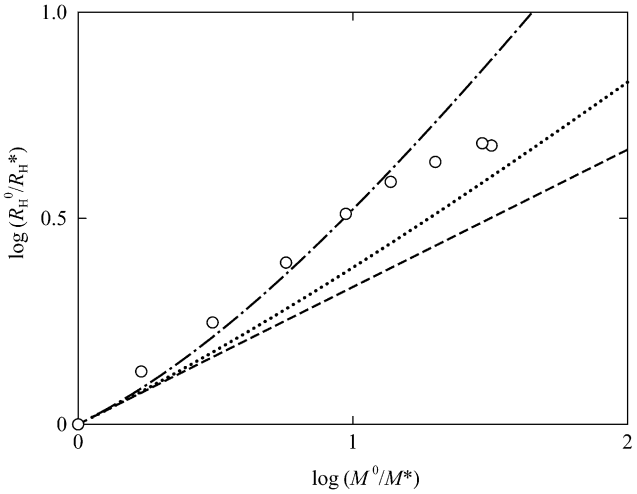

Fig. 12. Double-logarithmic plots of R_H^0/R_H^* against M^0/M^* for the present data (unfilled circles), and the theoretical results for rigid sphere (dashed line), prolate ellipsoid (dot dashed line), and oblate ellipsoid (dotted line).

4.2. Analysis of the R_H^0 vs. M^0 relation with wormlike spherocylinder model

The translational friction coefficient Ξ is calculated for the wormlike spherocylinder model with the total length L, the cross-sectional diameter d, and the stiffness parameter (or the Kuhn statistical length) λ^{-1} by Norisuye et al. [27]. Here the spherocylinder means a cylinder capped with hemispheres at its ends and thus becomes a sphere in the limit of $L = d$. Although the expression for Ξ is obtained only near the rod limit, it gives essentially the same results as those obtained from the Yamakawa et al.'s theory [28,29] for the wormlike cylinder model, except for small L/d. The latter theory ignores the end effects but is valid for any possible values of the model parameters. Thus, from these theories, we may derive the expression for R_H^0 as a function of L, d, and λ^{-1} over the entire range of L including the sphere, i.e. the case $L = d$. It reads

$$R_H^0 = \frac{L}{2f(\lambda L, \lambda d)} \tag{16}$$

The expression for the function f is so lengthy that we refer it to the original papers [27–29].

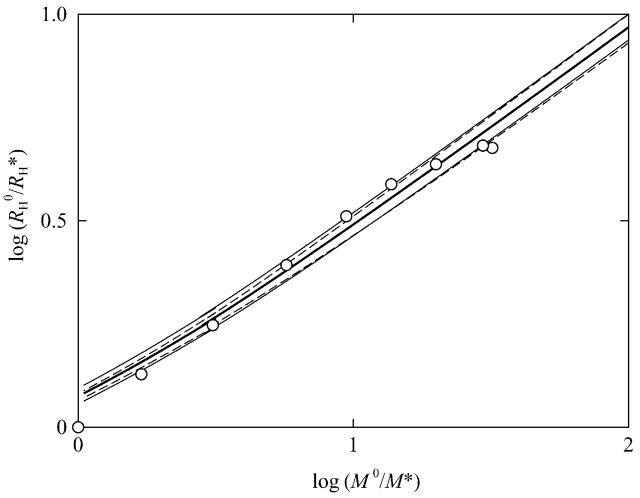

Fig. 13. Double-logarithmic plots of R_H^0/R_H^* against M_0/M^* for the present data (unfilled circles). The thick solid curve is a best-fit curve calculated by the use of the wormlike cylinder model, and the thin solid and dashed curves represent the allowances for the values of d and/or λ^{-1} (see text for details).

In the present analysis, we have calculated L from M^0 by the relation

$$L = \frac{4\nu M^0}{\pi N_A d^2} + \frac{d}{3} \tag{17}$$

where ν and d are again assumed to be independent of M^0 (or L). The theoretical values R_H^0/R_H^* have been calculated as a function of M^0/M^* for various values of λ^{-1} and d. Here R_H^* and M^* are the values of R_H^0 and M^0 for the sphere at $L = d$, respectively. Fig. 13 compares the observed and calculated results for R_H^0/R_H^* as a function of M^0/M^*. The thick solid line is a best-fit curve to the present experimental results, which yields a d value of 5.2 nm and a λ^{-1} value of 11.0 nm. It approximately describes the observed behavior of R_H^0, although the data points at the origin $W_0 = 0$ and at the largest M^0 ($W_0 = 10$) are deviated downward from the calculated line. The thin solid and dashed curves represent a tolerance of ± 0.2 nm of d at $\lambda^{-1} = 11.0$ nm and that of ± 2.0 nm of λ^{-1} at $d = 5.2$ nm, respectively. The present value of d is in good agreement with that determined at finite concentration from SANS measurements at large values of the scattering vector by Schurtenberger et al. [8,9]. This agreement indicates that the value of d is independent of lecithin concentration. On the other hand, our result for λ^{-1} is almost half of their value obtained from the SANS scattering functions. This difference is not explained at present.

In order to visualize the structure of the lecithin reverse micelles, we have calculated the L values at each W_0 by Eq. (17) from the values of M^0 given in Table 1 together with those of d(= 5.2 nm) and ν(= 0.982 cm^3/g) determined from Eq. (9). Then we have evaluated the cross-sectional diameter d_W of water core from the volume of water contained in the micelles calculated from the values of M^0 and W_0 with the value of specific volume of water (=1.003 cm^3/g at 25.0 °C), provided that the water core assumes a wormlike cylinder with total length L. The results are given in Table 3, in which the values of the thickness d_{PC} of lecithin shell covering the water core, the surface area S_s per lecithin molecule, and the diameter d_s of the area are also included. The structure of the lecithin reverse micelle is schematically drawn in Fig. 14.

Table 3
Values of the spherocylinder model parameters for lecithin reverse micelles

W_0	L (nm)	d_W (nm)	d_{PC} (nm)	S_s (nm)^2	d_s (nm)
1	8.8	0.73	2.24	1.18	1.22
2	14.6	1.06	2.07	1.10	1.18
3	25.5	1.33	1.94	1.06	1.16
4	40.9	1.53	1.84	1.06	1.16
5	58.8	1.71	1.75	1.06	1.16
6	84.7	1.86	1.67	1.08	1.17
8	125	2.11	1.55	1.12	1.19
10	135	2.31	1.45	1.17	1.22

Salient features of the structure of the lecithin reverse micelles deduced from the parameter values in Table 3 are summarized as follows:

1. The micelle becomes progressively longer with increasing W_0. The L value goes up to over 130 nm at large W_0.
2. The d_W value increases with W_0 and tend to level off at large W_0. (The values of d_W at W_0 larger than 6 are in reasonable agreement with those determined by the SANS experiments [9].)
3. The d_{PC} value decreases with increasing W_0 and tends to level off at large W_0. The values of d_{PC} are rather small especially at large W_0, thereby suggesting that a lecithin molecule does not take a fully extended form in the micelle; the length of the fully extended hydrophobic tail of a lecithin molecule is approximately 1.8 nm and the total length of a lecithin molecule in that case is about 3.0 nm.
4. The value of d_s is essentially independent of W_0. The results indicate that the intermolecular distance between the hydrophobic tails of two adjacent lecithin molecules is kept constant at a value of ca. 1.2 nm irrespective of

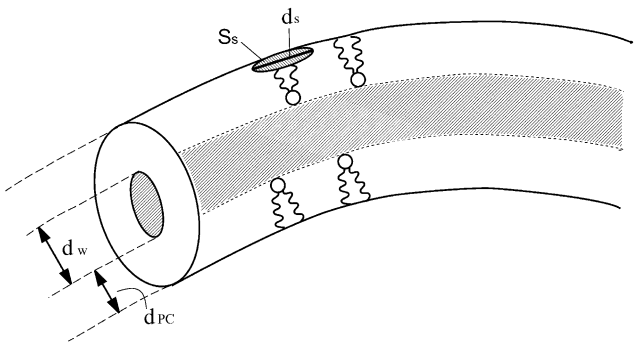

Fig. 14. Schematic drawing of the structure of the lecithin reverse micelle.

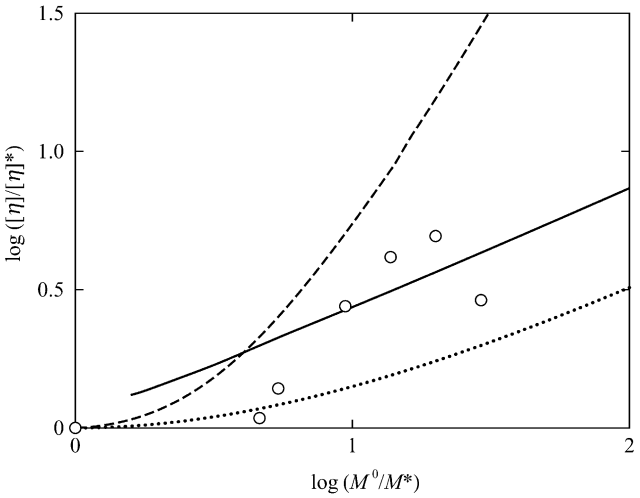

Fig. 15. Double-logarithmic plots of $[\eta]/[\eta]^*$ against M^0/M^* for the present data (unfilled circles and for the theoretical values for the wormlike spherocylinder model (solid curve), the prolate ellipsoid model (dashed curve), and the oblate ellipsoid model (dotted curve).

water content. In other words, the lecithin reverse micelles are formed and grow in the way that lecithin molecules are located at constant intervals in the micelle.

4.3. Intrinsic viscosity

In order to confirm the above analysis of R_H^0 with the wormlike spherocylinder model, we have investigated the intrinsic viscosity $[\eta]$ of the lecithin reverse micelles as a function of M^0. Fig. 15 compares the observed results (unfilled circles) with theoretical calculations (solid curve) obtained by the use of the same model and parameter values as above. Here, $[\eta]^*$ denotes the value of $[\eta]$ for the rigid sphere. In the theoretical calculations, we have used Yoshizaki et al.'s theory [30] for the wormlike touched-bead model which provides us with a formula applicable down to short and rather flexible chains pertinent to the present case. We note that no theory of $[\eta]$ is available for the wormlike spherocylinder model with small λL and large λd, but $[\eta]$ of the touched-bead model with the bead diameter taken as $d/0.74$ is shown to coincide with $[\eta]$ of the cylinder model in the range of large L. Therefore, the values of $[\eta]$ calculated above may be regarded as those for the wormlike spherocylinder model.

In Fig. 15 are also included the $[\eta]$ values calculated for the prolate (dashed curve) and oblate (dotted curve) ellipsoids [31] for reference. Here, the axial ratio P was converted to M^0 as described earlier. The data points do not follow either of the curves for the two types of ellipsoids, showing that neither one is an adequate model to the lecithin reverse micelles.

It is seen that they are located around the theoretical curve for the wormlike spherocylinder model, although the data are somewhat erroneous and the agreement between the observed and calculated results is rough. Thus, we may say that the results support the analysis of R_H^0 with the use of the wormlike spherocylinder model given in Section 4.2.

4.4. Micellar shape at finite concentrations

The lecithin reverse micelles at finite concentrations c possibly grow in both mass and size with increasing c accompanying the structural evolution. It is a difficult task to determine the molar mass M and the hydrodynamic radius R_H of the micelles independently by distinguishing between the contributions from concentration-dependent micellar growth and intermicellar interactions to the scattering results as mentioned in Section 1. For example, M in Eq. (11) should be in general taken to be a function of c and thus cannot be determined solely from the SLS results for $Kc/\Delta R_0$. The diffusion coefficient D obtained by Eq. (3) also includes the contributions from the hydrodynamic and thermodynamic interactions among micelles. To circumvent the difficulty, we here resort to combining information from DLS and SLS experiments.

In general, the mutual diffusion coefficient D determined by Eq. (3) is described by [32]

$$D = \frac{(1 - vc)M}{N_A \zeta}\left(\frac{\partial \pi}{\partial c}\right)_{T,p} \tag{18}$$

where ζ is the translational friction coefficient of a diffusing particle (or a micelle). Defining the hydrodynamic radius R_H (at finite concentrations) according to the Stokes law as

$$\zeta = 6\pi\eta_0 R_H \tag{19}$$

we obtain

$$D = \frac{(1 - vc)M}{6\pi\eta_0 N_A R_H}\left(\frac{\partial \pi}{\partial c}\right)_{T,p} \tag{20}$$

from Eq. (18). Note that Eq. (20) reduces to the Stokes–Einstein relation, i.e. Eq. (10), at $c = 0$. In this work, we have evaluated the ratio R_H/M by Eq. (20) from the DLS data for D determined by Eq. (3) and the SLS data for $(\partial\pi/\partial c)_{T,p}$ determined by Eq. (6), as previously done by Richtering et al. [33].

Fig. 16 shows the concentration dependence of R_H/M at various water content W_0 ranging from 0 to 10. Here the values of R_H/M on the ordinate axis are reduced by their respective values at $c = 0$, i.e. R_H^0/M^0. It is found that at any fixed value of W_0, R_H/M increases with increasing c, following a curve concave upward to a greater extent for larger W_0. While the value of R_H/M at the highest c examined is about 3.5 times that of R_H^0/M^0 at $W_0 = 0$, the increase of R_H/M at $W_0 = 10$ is much greater, amounting to a value of ca. 10 times that of R_H^0/M^0 at the highest c examined. The variation of R_H/M with c may be attributed to the following changes in the lecithin reverse micelles:

1. micellar growth in mass or increase of M
2. micellar growth in size or increase of R_H

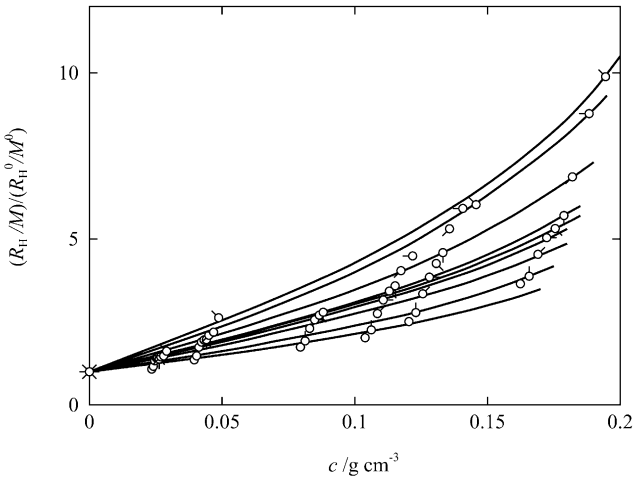

Fig. 16. Concentration c dependence of R_H/M of the lecithin reverse micelles at various values of W_0. The ordinate quantity is reduced by the value at $c = 0$. Symbols have the same meaning as those in Fig. 7.

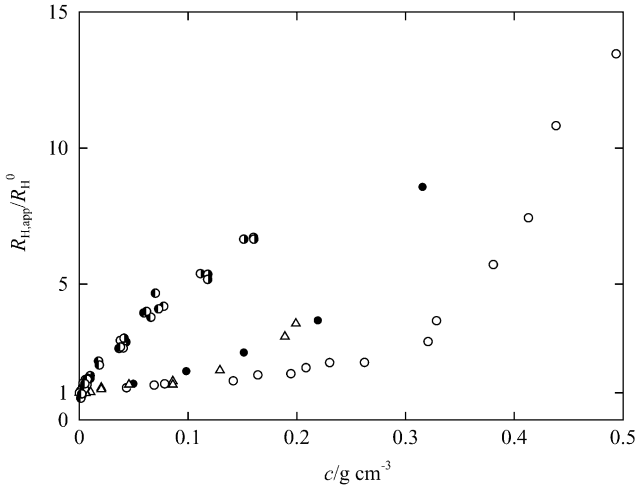

Fig. 17. Concentration c dependence of the apparent hydrodynamic radius $R_{H,app}$ for colloidal particles (unfilled circles) [34], human hemoglobin (filled circles) [35], bovine serum albumin (triangle) [35], and poly(γ-benzyl α,L-glutamate) (right-half-filled circles, $P = 26$ left-half-filled circles, $P = 63$) [36]. Here, $R_{H,app}$ on the ordinate axis is reduced by the value R_H^0 at $c = 0$.

3. change in the micellar shape, e.g. from sphere to cylinder or from short cylinder to long one.

The effect (1) decreases the values of R_H/M and the latter two effects increase them. In addition to these effects, the hydrodynamic interaction among the micelles may contribute to the increase of R_H/M with increasing c. It is considered that the behavior of R_H/M found in Fig. 16 results from the contribution grouped these effects.

In order to interpret the results shown in Fig. 16 at least qualitatively, we have culled from the literature the experimental data on the apparent hydrodynamic radius $R_{H,app}$ as a function of c for rigid particles or molecules. Here, we have chosen, to examine the effect of the hydrodynamic interaction on $R_{H,app}$ for the particles of definite shape with various axial ratios P, the results for colloid particles (sphere, $P = 1$) [34], human hemoglobin (prolate ellipsoid, $P = 2$–4) [35], bovine serum albumin (prolate ellipsoid, $P = 3$–4) [35], obtained by tracer diffusion studies, and poly(γ-benzyl α,L-glutamate) in a helicogenic solvent (cylinder, $P = 26$ and 63) [36] obtained by DLS studies combined with SLS experiments. The literature results are depicted in Fig. 17, in which the values of $R_{H,app}$ reduced by the respective infinite-dilution values R_H^0 are plotted against c. It should be noted that the increases of $R_{H,app}$ found in this figure result solely from the hydrodynamic interaction among solute particles. We find that in the range of c corresponding to the region of Fig. 16, i.e. $0 \le c < 0.2$ g/cm^3, $R_{H,app}$ for the rigid sphere only moderately increases with c and $R_{H,app}$ for the biological molecules increases more significantly to a greater extent for larger P.

For the lecithin reverse micelles at infinite dilution, we may calculate the values of P from the L and d values determined above as, e.g. $P = 1$ at $W_0 = 0$, $P = 4.9$ at $W_0 = 3$, and $P = 26$ at $W_0 = 10$. Fig. 16 demonstrates that the values of R_H/R_H^0 at $W_0 = 0$, 3, and 10 go up to ca. 3.6, 5.0, and 10, respectively, at the highest c examined, provided that M at each W_0 remains constant in the range of c. If we take into account the possible increase of M, the increases of R_H/R_H^0 are anticipated to be much larger. They are definitely larger than those for the corresponding P values found in Fig. 17. Although parts of them are attributed to the effect of the hydrodynamic interaction among micelles, the present results for the increase of R_H in Fig. 16 are not entirely explained only by the hydrodynamic interaction among micelles. We may, therefore, conclude that the lecithin reverse micelles change their shape with increasing c in such a way as from sphere to cylinder at $W_0 = 0$ and from short cylinder to longer one at higher W_0. The conclusion is, however, rather speculative at present. In order to attain definitive conclusions, we may have to determine M at finite concentrations.

5. Concluding remarks

In this work, we have characterized the lecithin reverse micelles with and without containing water in cyclohexane at 25.0 °C. We have determined the molar mass M^0 and the hydrodynamic radius R_H^0 of the micelles at infinite dilution by extrapolating the SLS results $Kc/\Delta R_0$ and the mutual diffusion coefficient D from DLS measurements to $c = 0$. Both M^0 and R_H^0 have increased with increasing water content W_0, thereby indicating that the micelles grow in mass and in size with water uptake into them. This may be the first time that the micellar growth has been unequivocally demonstrated by the experimental observations.

The data of R_H^0 as a function of M^0 has been successfully analyzed with the use of the wormlike spherocylinder model, yielding a value of the stiffness parameter λ^{-1} of

11.0 nm and that of the cross-sectional diameter of 5.2 nm. The analysis has also given the values of the cross-sectional diameter of water core d_W and the thickness of lecithin shell d_{PC} as a function of W_0. The results have revealed that the lecithin reverse micelles assume a shape of rather flexible cylinder at finite W_0, while they are spherical at $W_0 = 0$. It has been shown from the structure of the micelle and the number of lecithin molecules in it that the intermolecular distance between hydrophobic tails of two adjacent lecithin molecules on the micellar surface remains constant at a value of ca. 1.2 nm irrespective of water content W_0. This may provides us with an information about formation and growth of the lecithin reverse micelles in the present system.

The results for the ratio of the hydrodynamic radius R_H to the molar mass M, i.e. R_H/M, of the micelles at finite concentration c have shown that the lecithin reverse micelles grow with increasing c, accompanying changes in shape; the micellar shape changes from sphere to cylinder at $W_0 = 0$ and from short to long cylinder at finite W_0. This conclusion is not, however, definitive as yet, since the effects of the increase of M and of the hydrodynamic interaction of R_H with increasing c are still included in the results for R_H/M. In order to observe the micellar growth at finite c more clearly, we have to determine R_H and M independently. To accomplish this, we may need a molecular thermodynamic theory developed for the model appropriate to elucidate the formation and growth of the micelles. We leave it for future work.

Acknowledgements

This research was supported in part by a Grant-in-Aid (11450368) from the ministry of Education, Science, and Culture, Japan.

References

[1] Schurtenberger P, Scartazzini R, Magid LJ, Leser ME, Luisi PL. J Phys Chem 1990;94:3695.
[2] Schurtenberger P, Peng Q, Leser ME, Luisi PL. J Colloid Interface Sci 1993;156:43.
[3] Angelico R, Ceglie A, Olsson U, Palazzo G. Langmuir 2000;16:2124.
[4] Schurtenberger P, Cavaco C. J Phys I 1993;3:1279.
[5] Schurtenberger P, Cavaco C. Langmuir 1994;10:100.
[6] Schurtenberger P, Cavaco C. J Phys Chem 1994;98:5481.
[7] Lin T-L, Hu Y, Liu W-J. Langmuir 1997;13:1422.
[8] Schurtenberger P, Magid LJ, King SM, Lindner P. J Phys Chem 1991;95:4173.
[9] Schurtenberger P, Jerke G, Cavaco C, Pederson JS. Langmuir 1996;12:2433.
[10] Jerke G, Pederson JS, Egelhaaf SU, Schurtenberger P. Phys Rev E 1997;56:5772.
[11] Scartazzini R, Luisi PL. J Phys Chem 1988;92:829.
[12] Schurtenberger P, Scartazzini R, Luisi PL. Rheol Acta 1989;28:372.
[13] Shchipunov YA, Hoffmann H. Langmuir 1998;14:6350.
[14] Shchipunov YA, Hoffmann H. Langmuir 1999;15:7108.
[15] Mezzasalma SA, Koper GJM, Shchipunov YA. Langmuir 2000;16:10564.
[16] Angelico R, Palazzo G, Colafemmina G, Cirkel PA, Ginstini M, Ceglie A. J Phys Chem 1998;102:2883.
[17] Angelico R, Balinov B, Ceglie A, Olsson U, Palazzo G, Soderman O. Langmuir 1999;15:1679.
[18] Koppel OE. J Chem Phys 1972;57:4817.
[19] Yamada T, Koyama H, Yoshizaki T, Einaga Y, Yamakawa H. Macromolecules 1993;26:2566.
[20] Provencher SW. Makromol Chem 1979;180:201.
[21] Pike ER, Pomeroy RM, Vaughan JM. J Chem Phys 1975;62:3188.
[22] Einaga Y, Mitani T, Hashizume J, Fujita H. Polym J 1979;11:565.
[23] Casassa EF, Berry GC. In: Allen G, editor. Comprehensive polymer science, vol. 2. New York: Pergamon Press, 1988. Chapter 3; and references cited therein.
[24] Einaga Y, Abe F, Yamakawa H. J Phys Chem 1992;96:3948.
[25] Weisberger A, Proskauer ES, Riddick JA, Toops Jr EE. Organic solvents. 2nd ed. New York: Interscience, 1955.
[26] Probstein RF. Physicochemical hydrodynamics. 2nd ed. New York: Wiley, 1994.
[27] Norisuye T, Motowoka M, Fujita H. Macromolecules 1979;12:320.
[28] Yamakawa H, Fujii M. Macromolecules 1973;6:407.
[29] Yamakawa H, Yoshizaki T. Macromolecules 1979;12:32.
[30] Yoshizaki T, Nitta I, Yamakawa H. Macromolecules 1988;21:165.
[31] Frisch HL, Simha R. In: Eirich FR, editor. Rheology, vol. 1. New York: Academic Press, 1956. Chapter 14.
[32] Yamakawa H. Modern theory of polymer solutions. New York: Harper & Row, 1971.
[33] Richtering WH, Burchard W, Jahns E, Finkelmann H. J Phys Chem 1988;92:6032.
[34] van Megen W, Underwood SM. Langmuir 1990;6:35.
[35] Phillies GDJ. Macromolecules 1986;19:2367.
[36] DeLong LM, Russo PS. Macromolecules 1991;24:6139.